

Monte Carlo study of charge transport in organic sandwich-type single-carrier devices: Effects of Coulomb interactions

J. J. M. van der Holst,^{1,*} F. W. A. van Oost,¹ R. Coehoorn,^{2,3} and P. A. Bobbert¹

¹*Theory of Polymers and Soft Matter, Department of Applied Physics, Eindhoven University of Technology, P.O. Box 513, NL-5600 MB Eindhoven, The Netherlands*

²*Philips Research Laboratories Eindhoven, High Tech Campus 4, NL-5656 AE Eindhoven, The Netherlands*

³*Group Molecular Materials and Nanosystems, Department of Applied Physics, Eindhoven University of Technology, P.O. Box 513, NL-5600 MB Eindhoven, The Netherlands*

(Received 30 July 2010; published 22 February 2011)

We present the results of Monte Carlo simulations of transport of charge carriers of a single type in devices consisting of a disordered organic semiconductor sandwiched in between two electrodes. The simulations are based on hopping of carriers between sites with a Gaussian energetic distribution, which is either spatially uncorrelated or has a correlation based on interactions with randomly oriented dipoles. Coulomb interactions between the carriers are taken into account explicitly. For not too small injection barriers between the electrodes and the organic semiconductor, we find that the current obtained from the simulations can be described quite well by a one-dimensional drift-diffusion continuum model, which takes into account the long-range contributions of Coulomb interactions through the space-charge potential. For devices with low injection barriers, however, the simulations yield a considerably lower current than the continuum model. The reduction of the current for uncorrelated disorder is larger than for correlated disorder. By performing simulations in which the short-range contributions of the Coulomb interactions between the carriers are omitted, we demonstrate that the difference is caused by these short-range contributions. We can rationalize our results by analyzing the three-dimensional current distributions and the in-plane radial distribution function of the carriers resulting from the simulations for different injection barriers with and without taking into account these short-range contributions.

DOI: [10.1103/PhysRevB.83.085206](https://doi.org/10.1103/PhysRevB.83.085206)

PACS number(s): 85.30.De, 72.20.Ee, 72.80.Le, 72.80.Ng

I. INTRODUCTION

Organic light-emitting diodes (OLEDs) are promising high-efficiency light sources that are presently used in a variety of lighting and display applications. They consist of one or more layers of organic semiconducting material sandwiched in between electrodes, of which one is usually a low-work-function metal and the other a transparent conducting oxide such as indium tin oxide. Despite the growing commercial success of OLEDs, knowledge of many aspects of their functioning is still fragmental.

One of the most important of these aspects is the charge transport. It has become clear in the past two decades that disorder plays a very important role in charge transport because it leads to the localization of electronic states. The transport is assumed to take place by hopping of carriers between the sites at which the states are localized. The energetic disorder is often modeled by assuming that the on-site energies are random variables, taken from a Gaussian density of states (DOS), resulting in what has been called the Gaussian disorder model (GDM). The dependence of the charge-carrier mobility μ on temperature and electric field in the GDM was investigated by Bässler *et al.* using Monte Carlo (MC) simulations of the hopping transport of a single carrier in a Gaussian DOS.^{1,2}

Gartstein and Conwell suggested that spatial correlation in the disorder should be included to better describe experimental charge-transport data. These data show a mobility μ with a Poole-Frenkel dependence on the electric field, $\mu \propto \exp[\gamma\sqrt{F}]$, in a rather wide range of electric-field strengths F , with γ a factor depending on temperature.³ In

particular, it was suggested that the fields of randomly oriented dipoles could be the origin of such correlated disorder.^{4,5} The resulting model is known as the correlated disorder model (CDM).

In addition, the dependence of the mobility on the carrier density has to be accounted for at densities where state-filling effects become important.^{6,7} For such densities, the independent-carrier assumption in the MC simulations of Bässler *et al.*,^{1,2} also called the Boltzmann limit, is invalid. The mobility increases with increasing density, because the occupation of the lowest-energy states by carriers reduces the effect of these states as trapping centers. Pasveer *et al.*⁸ performed a computational study—involving a solution of the Pauli master equation for the occupational probabilities of a cubic array of hopping sites—of the dependence of the mobility on temperature, electric field, and carrier density in the case of a spatially uncorrelated Gaussian DOS. It was shown that the mobility obtained from that study can provide an excellent quantitative explanation of measured current-voltage characteristics of hole-only devices of two derivatives of the semiconducting polymer poly(*p*-phenylenevinylene) (PPV),⁸ as well as a derivative of polyfluorene.⁹ It was found that in these devices at room temperature the density dependence of the hole mobility is more important than the field dependence. We will refer to this extension of the GDM, regarding the inclusion of the density dependence of the mobility, as the extended Gaussian disorder model (EGDM).

For the case of a spatially correlated Gaussian DOS, a similar computational study of the density dependence of the mobility was performed by Bouhassoune *et al.*¹⁰ We

will refer to this extension of the CDM as the extended correlated disorder model (ECDM). A comparison of EGDM and ECDM modeling of current-voltage characteristics of hole-only devices of conjugated polymers such as derivatives of PPV¹⁰ and a polyfluorene-based copolymer¹¹ has led to the conclusion that for these polymers the intersite distance as obtained from a fit of the EGDM modeling is more realistic than the one obtained from a fit of the ECDM modeling. On the other hand, a similar comparison of EGDM and ECDM modeling of current-voltage characteristics of hole-only devices of the molecule *N,N'*-bis(1-naphthyl)-*N,N'*-diphenyl-1,1'-biphenyl-4,4'-diamine (α -NPD) and of electron-only devices of the molecule bis(2-methyl-8-quinolinolato)(4-phenylphenolato) aluminum (BALq) shows that the intersite distance as obtained from a fit with the ECDM modeling is more realistic than the one obtained with the EGDM modeling.^{12,13} This work suggests that for the investigated polymers and small-molecule semiconductors the EGDM and the ECDM, respectively, are thus the best models to describe charge transport.

In the above device-modeling studies within the EGDM and ECDM, a one-dimensional (1D) continuum drift⁸ or drift-diffusion equation^{9,14} was solved using a mobility with a parametrization of the dependence on temperature, electric field, and carrier density based on a numerical solution for the mobility obtained by solving the Pauli master equation for the site-occupational probabilities.^{8,10} In order to investigate the consistency of this approach and to study the injection of carriers in more detail, we recently performed a computational study of single-carrier devices by solving the Pauli master equation for a collection of sites representing a full three-dimensional (3D) device, including its electrodes.¹⁵ The DOS was taken to be Gaussian and to be spatially uncorrelated, corresponding to the EGDM. The effects of space charge, the image-charge potential, and an injection barrier were taken into account. The space charge was taken into account in a layer-averaged way, neglecting any explicit short-range Coulomb interactions between charges. The image-charge potential was taken into account by including the Coulomb interaction between a charge and its image charge when it is close to one of the electrodes.

In these 3D device studies,¹⁵ the current density was found to be highly inhomogeneous, in agreement with other studies.¹⁶⁻¹⁹ This inhomogeneous structure involves narrow current filaments that carry almost all the current, characteristic of the percolative nature of charge transport in disordered materials. Despite these 3D inhomogeneities, the current-voltage characteristics were found to be described quite well by the 1D continuum drift-diffusion device model of Ref. 14, with an image-charge-induced lowering of the injection barrier included in a similar way as in the work of Emtage and O'Dwyer.²⁰ For thin devices and high disorder strengths the current obtained from the 3D calculations was found to be somewhat higher than that obtained from the 1D drift-diffusion model. It is in this regime that the current density becomes extremely nonuniform. It was found that in this regime the current-voltage characteristics can be described rather well with a model of Burin and Ratner, which assumes injection of carriers along 1D current pathways.²¹

While the above 3D device studies properly take into account the effects of percolation, the effects of Coulomb interactions between the carriers are only taken into account in an average way by evaluating a layer-averaged space charge. In fact, the short-range effects of Coulomb interactions between carriers cannot be taken into account in a consistent way within the master-equation approach, because this approach involves the time-averaged and not the actual occupational probabilities of the sites. On the other hand, in MC simulations it is, in principle, straightforward to take the effects of Coulomb interactions fully into account. For a bulk organic semiconductor, these effects have recently been investigated using MC simulations by Zhou *et al.*²² Very important effects were found at a rather large electric field and high carrier densities ($>10^{-2}$ carriers per site), where Coulomb interactions were found to decrease the mobility at low disorder strength, but to increase the mobility at high disorder strength. However, also at low densities ($<10^{-2}$ carriers per site) influences of the Coulomb interactions were found. Therefore, it is important to study the effects of Coulomb interactions in devices where high carrier densities can be reached at the electrodes in the case of low injection barriers and where the carrier density can vary over several orders of magnitude within a distance of only a few nanometers from the electrodes. The effect of Coulomb interactions on transport across organic heterojunctions has been studied using MC simulations by Houili *et al.*²³ At these heterojunctions the carrier concentration can also become very large, leading to important effects of Coulomb interactions. Multiparticle MC simulation methods have also been used to study diffusion-limited recombination in polymer-fullerene blends.²⁴

Another reason to study the effects of Coulomb interactions explicitly is a double-counting problem that occurs when both the space charge and the image-charge potential are taken into account either in a 3D master-equation approach or in a 1D continuum drift-diffusion model. The problem is that, in taking into account the space charge and the correct boundary conditions for the electrostatic potential at the electrodes, the image-charge potential related to the space charge has already been taken into account. When considering a particular charge, it is therefore not consistent to take into account the interaction of this charge with its image charge, because the contribution of this charge to the space charge was already accounted for, albeit in an average way. It is not *a priori* clear what the size is of the error that is made by this double counting. The problem of taking into account the image-charge potential in a consistent way was recently discussed in detail by Genenko *et al.*²⁵ and in Secs. II B and III we will discuss this issue further. The problem can be obviously circumvented by performing MC simulations in which Coulomb interactions are taken into account explicitly.

In the present work we will show and discuss the results of MC simulations for single-carrier devices consisting of an organic semiconductor sandwiched in between two equal electrodes. We will take into account Coulomb interactions in the following way. Around every charge in the device a cutoff sphere is defined. Interactions with charges within this sphere are taken into account explicitly, while interactions with charges outside this sphere are taken into account in a layer-averaged way. With an optimal choice of the radius of the cutoff

sphere, we take into account the short-range as well as the long-range contributions of the Coulomb interactions in a proper way, while maintaining a sufficient computational efficiency. Moreover, by reducing the radius of the cutoff sphere to zero, we can study the situation where Coulomb interactions are only taken into account in a layer-averaged way, corresponding to the approximation made in the 3D master-equation approach and the 1D continuum drift-diffusion model.

The paper is set up as follows. Section II discusses the theory and the methods used. In Sec. II A we describe our MC approach and discuss in detail our method to take into account Coulomb interactions, which was briefly sketched in the previous paragraph. Section II B discusses the 1D drift-diffusion model used for calculating the current density in single-carrier devices. In Sec. III we present the current-voltage characteristics of devices with uncorrelated as well as correlated disorder, corresponding to the EGDM and ECDM, respectively. For the case of the EGDM, we compare our results with our previous work based on the master-equation approach,¹⁵ while for both the EGDM and the ECDM we compare our results with those of 1D drift-diffusion modeling. In Sec. IV we show plots of the 3D current density in devices with correlated and uncorrelated disorder, with and without taking into account the short-range contributions of the Coulomb interactions. We also show the in-plane radial distribution functions of the carriers in the first organic layer close to the injecting electrode and in the middle organic layer. These results allow us to rationalize the effects of short-range Coulomb interactions. Section V contains a summary and conclusions.

II. THEORY AND METHODS

A. Monte Carlo method

In this section we describe our MC approach for calculating the current density in a single-carrier device consisting of an organic semiconducting material sandwiched in between two electrodes. The organic semiconductor and the electrodes are modeled by a 3D cubic $m_x \times m_y \times m_z$ lattice with lattice constant a . A lattice site is denoted by $\mathbf{i} = \{i_x, i_y, i_z\}$. The sites with $i_x = 1$ and $i_x = m_x$ represent the injecting and collecting electrodes, respectively. The other sites, which we call “organic” sites, represent localized electronic states in the organic semiconductor. Periodic boundary conditions are taken in the y and z directions. The applied electric field is in the x direction.

We assume that the hopping of charge carriers from one site to another is a thermally assisted tunneling process with a coupling to an acoustical phonon bath. The hopping rate W_{ij} from site \mathbf{i} to \mathbf{j} is then described by the Miller-Abrahams formalism,²⁶

$$W_{ij} = v_0 \exp \left[-2\alpha |\mathbf{R}_{ij}| - \frac{\Delta E_{ij}}{k_B T} \right] \quad \text{for } \Delta E_{ij} > 0, \quad (1a)$$

$$W_{ij} = v_0 \exp [-2\alpha |\mathbf{R}_{ij}|] \quad \text{for } \Delta E_{ij} \leq 0, \quad (1b)$$

where v_0 is an intrinsic rate, α is the inverse localization length of the localized wave functions, $|\mathbf{R}_{ij}|$ is the distance between sites \mathbf{i} and \mathbf{j} , k_B is Boltzmann’s constant, T is the temperature, and ΔE_{ij} is the difference $E_j - E_i$ between the on-site energies of sites \mathbf{j} and \mathbf{i} . The on-site energy E_i of an organic

site is equal to the sum of a random on-site energy contribution $E_{\text{rand},i}$, an electrostatic contribution $e\Phi_{\text{applied},i}$ owing to the applied potential, a contribution $e\Phi_{\text{self},i}$ owing to the Coulomb interactions of a charge with its own (repetitive) image charges, and a contribution $e\Phi_{\text{interact},i}$ owing to Coulomb interactions of a charge with all other charges and their image charges.

We assume that the hopping rate of a charge carrier from an electrode site to an organic site and vice versa is described by the same expression [Eq.(1)] as the mutual hopping rate between organic sites. It is to be expected that the specific form of this hopping rate has almost no influence on the current-voltage characteristics, as long as there is a thermal equilibrium between the electrode and the adjacent organic sites. We model injection and collection by the electrodes by assuming that there is always a carrier at an electrode site ready to hop to an adjacent empty organic site, and that a carrier at an organic site can always hop to an adjacent electrode site. When a charge hops from the injecting or collecting electrode to an organic site, it will experience an injection barrier, Δ_1 or Δ_2 , respectively. To take this into account in Eq.(1), we then use $\Delta E_{ij} = E_j + \Delta_1$ or $\Delta E_{ij} = E_j + \Delta_2$ when a charge hops from the injecting electrode ($i_x = 1$) or collecting electrode ($i_x = m_x$), respectively, to an organic site. A similar change is made for hopping from an organic site into one of the electrodes.

We consider the situations of spatially uncorrelated as well as spatially correlated disorder. In the case of spatially uncorrelated disorder, the energies $E_{\text{rand},i}$ are randomly drawn from a Gaussian DOS:

$$g(E) = \frac{1}{\sqrt{2\pi}\sigma a^3} \exp \left[-\frac{E^2}{2\sigma^2} \right], \quad (2)$$

with σ the width of this DOS. For the electrode sites we set these energies equal to 0. In the case of spatially correlated disorder, we take the energy $E_{\text{rand},i}$ at site \mathbf{i} equal to the electrostatic energy resulting from permanent random dipoles \mathbf{d}_j of equal magnitude d but random orientation on all the other organic sites $\mathbf{j} \neq \mathbf{i}$. The resulting DOS is Gaussian, with a width σ proportional to d .^{5,27,28} The on-site energy $E_{\text{rand},i}$ is then given by

$$E_{\text{rand},i} = - \sum_{\mathbf{j} \neq \mathbf{i}} \frac{e\mathbf{d}_j \cdot \mathbf{R}_{ij}}{\epsilon_0 \epsilon_r |\mathbf{R}_{ij}|^3}, \quad (3)$$

with the sum over all sites \mathbf{j} in a sufficiently large box around site \mathbf{i} , e the unit charge, ϵ_0 the vacuum permittivity, and ϵ_r the relative dielectric constant of the organic material. The resulting disorder strength is then given by $\sigma \approx 2.35(ed)/(\epsilon_0 \epsilon_r a^2)$. The dimensionless correlation function $C(r)$ between the on-site energies is defined by

$$C(r = |\mathbf{R}_{ij}|) \equiv \frac{\langle E_{\text{rand},i} E_{\text{rand},j} \rangle}{\sigma^2}, \quad (4)$$

in which $\langle \dots \rangle$ denotes an ensemble average over different random configurations of the dipole orientations. The correlation function is at an intersite distance $r = a$ equal to $C(r = a) \approx 0.7$, at $r = 2a$ equal to $C(r = 2a) \approx 0.35$, and for larger intersite distances equal to $C(r = |\mathbf{R}_{ij}|) \approx 0.74a/|\mathbf{R}_{ij}|$.²⁹

We also looked at the effects of image dipoles. To take image dipoles into account we consider the $m_x \times m_y \times m_z$

lattice of random dipoles. A dipole $\mathbf{d}_i = \{d_{i,x}, d_{i,y}, d_{i,z}\}$ on site $\mathbf{i} = \{i_x, i_y, i_z\}$ will have image dipoles $\mathbf{d}_{\text{odd},i} = \{d_{i,x}, -d_{i,y}, -d_{i,z}\}$ on the sites given by $\mathbf{i}_{\text{odd},n} = \{-i_x + 2nm_x, i_y, i_z\}$ outside the device and image dipoles $\mathbf{d}_{\text{even},i} = \{d_{i,x}, d_{i,y}, d_{i,z}\}$ on the sites given by $\mathbf{i}_{\text{even},n} = \{i_x + 2nm_x, i_y, i_z\}$ outside the device, with n an integer. Note that the original dipole is located at $\mathbf{i}_{\text{even},0}$. The random on-site energy $E_{\text{rand},i}$ is then given by

$$E_{\text{rand},i} = - \sum_{\mathbf{j} \neq \mathbf{i}} \frac{e\mathbf{d}_j \cdot \mathbf{R}_{ij}}{\epsilon_0 \epsilon_r |\mathbf{R}_{ij}|^3} - \sum_{n=-n_{\text{images}}}^{n_{\text{images}}} \frac{e\mathbf{d}_{\text{odd},j} \cdot \mathbf{R}_{ij_{\text{odd},n}}}{\epsilon_0 \epsilon_r |\mathbf{R}_{ij_{\text{odd},n}}|^3} - \sum_{n=-n_{\text{images}}, n \neq 0}^{n_{\text{images}}} \frac{e\mathbf{d}_{\text{even},j} \cdot \mathbf{R}_{ij_{\text{even},n}}}{\epsilon_0 \epsilon_r |\mathbf{R}_{ij_{\text{even},n}}|^3}, \quad (5)$$

where the first term is equal to Eq. (3) and the second and third terms give the contributions of the image dipoles. It is sufficient to take $n_{\text{images}} = 1$ for the devices studied in this paper.

The Fermi energy in the collecting electrode is taken as the zero-energy reference value, so that the electrostatic contribution owing to the applied potential, $e\Phi_{\text{applied},i}$, at the injecting and collecting electrode is given by $e\Phi_{\text{applied},\{i_x=1, i_y, i_z\}} = eV$ and $e\Phi_{\text{applied},\{i_x=m_x, i_y, i_z\}} = 0$, respectively, with V the applied driving voltage. $e\Phi_{\text{applied},i}$ at the organic sites is determined by a linear drop of the potential over the device.

A charge on an organic site will experience an interaction with its repetitive image charges with alternating sign in the two conducting electrodes. Up to order n_{images} the contribution owing to the Coulomb interactions of a charge with its image charges, $e\Phi_{\text{self},i}$, is given by

$$e\Phi_{\text{self},i} = - \frac{e^2}{16\pi\epsilon_0\epsilon_r a} \left(\sum_{n=-n_{\text{images}}}^{n_{\text{images}}} \frac{1}{2i_x + 2nm_x} - \sum_{n=-n_{\text{images}}, n \neq 0}^{n_{\text{images}}} \frac{1}{2nm_x} \right) \quad (6)$$

at the organic sites. Because of the translational symmetry in the y and z directions, $e\Phi_{\text{self},i}$ only depends on the layer index i_x . In our simulations we took $n_{\text{images}} = 100$, which is more than sufficient.

The on-site energy E_i also contains the Coulomb interaction energy $e\Phi_{\text{interact},i}$ with all the other charges and the image charges of these other charges. For practical reasons we split $e\Phi_{\text{interact},i}$ into three contributions. (1) First, we take into account a short-range contribution $e\Phi_{\text{sr},i}$, in which the Coulomb interaction energy with charges within a sphere of radius R_c is taken into account explicitly. (2) Next, we add a layer-averaged contribution $e\Phi_{\text{layer},i}$, in which the Coulomb interaction energy with the other charges is taken into account in a layer-averaged way. Because this contribution also takes into account the layer-averaged Coulomb energy of charges in the disk-shaped parts of the layers within the sphere, a double counting occurs. (3) Therefore, we subtract a contribution $e\Phi_{\text{disks},i}$ to correct for this double counting. By increasing R_c we can systematically investigate the effect of taking into account the short-range contributions of the Coulomb interactions. For $R_c = 0$, Coulomb interactions of a charge with other charges and their image charges are only taken into account in a layer-averaged way while the interaction of a charge with its own image charges is taken into account explicitly, as in our previous master-equation calculations.¹⁵ With increasing R_c , Coulomb interactions are taken into account in an increasingly exact way, with full exactness for $R_c = \infty$. For a well-chosen finite value of R_c we can obtain a good compromise between accuracy and simulation speed. For the device simulations discussed in Secs. III and IV, we have taken $R_c = 10a$, which yields sufficient accuracy.

The short-range contribution of the Coulomb potential at site $\mathbf{i} = \{i_x, i_y, i_z\}$, owing to a charge at site $\mathbf{j} = \{j_x, j_y, j_z\}$ and its image charges is given, up to order n_{images} , by

$$f_{c,i,j} = \begin{cases} \frac{e}{4\pi\epsilon_0\epsilon_r a} \left(\frac{1}{|\mathbf{R}_{ij}|} - \sum_{n=-n_{\text{images}}}^{n_{\text{images}}} \frac{1}{\sqrt{(j_x + i_x + 2nm_x)^2 + (j_y - i_y)^2 + (j_z - i_z)^2}} \right. \\ \left. + \sum_{n=-n_{\text{images}}, n \neq 0}^{n_{\text{images}}} \frac{1}{\sqrt{(j_x - i_x + 2nm_x)^2 + (j_y - i_y)^2 + (j_z - i_z)^2}} \right), & |\mathbf{R}_{ij}| \leq R_c, \\ 0, & |\mathbf{R}_{ij}| > R_c. \end{cases} \quad (7)$$

The interaction energy $e\Phi_{\text{sr},i}$ is then obtained as

$$e\Phi_{\text{sr},i} = \sum_{\mathbf{j} \neq \mathbf{i}} e_j f_{c,i,j}, \quad (8)$$

with $e_j = e$ when a charge is present at site \mathbf{j} and $e_j = 0$ otherwise. In our simulations we also took $n_{\text{images}} = 100$ in Eq. (7).

In order to calculate the layer-averaged electrostatic contribution $e\Phi_{\text{layer},i}$, the Poisson equation is solved with the layer-averaged charge density ρ_{j_x} , in each layer j_x as a source term. Consequently, $e\Phi_{\text{layer},i}$ depends only on the layer index i_x . owing to the image-charge contribution, $e\Phi_{\text{layer},i}$ is zero at both the injecting and collecting electrode sites.

Finally, we have to calculate the double-counting correction $e\Phi_{\text{disks},i}$, owing to the average charge in the disks in each layer j_x formed by the intersection between the sphere with radius R_c centered around site \mathbf{i} and the layer j_x . These disks have the

same layer-averaged charge density ρ_{j_x} as the layer j_x in which they are located. The potential at site \mathbf{i} of the disk in layer j_x , up to order n_{disks} images of the disks, is given by

$$f_{\text{disk},i_x,j_x} = \begin{cases} \frac{\rho_{j_x}}{2\epsilon_0\epsilon_r} \left(\sqrt{R_{j_x-i_x}^2 + a^2(j_x - i_x)^2} - a|j_x - i_x| \right. \\ \quad - \sum_{n=-n_{\text{disks}}}^{n_k} \left\{ \sqrt{R_{j_x-i_x}^2 + a^2(j_x + i_x + 2nm_x)^2} \right. \\ \quad \left. - a|j_x + i_x + 2nm_x| \right\} \\ \quad + \sum_{n=-n_{\text{disks}}, n \neq 0}^{n_{\text{disks}}} \left\{ \sqrt{R_{j_x-i_x}^2 + a^2(j_x - i_x + 2nm_x)^2} \right. \\ \quad \left. - a|j_x - i_x + 2nm_x| \right\} \Big), & 0 < a|j_x - i_x| \leq R_c, \\ 0, & a|j_x - i_x| > R_c, \end{cases} \quad (9)$$

with $R_{j_x-i_x} = \sqrt{R_c^2 - a^2(j_x - i_x)^2}$ the radius of the disk in layer j_x . We note that in Eq. (9) the Coulomb potential of a continuous disk-shaped charge distribution is calculated, while in Eq. (7) the Coulomb potential of a discrete set of point charges is calculated. The error as a result of the mismatch of these two potentials becomes smaller when R_c becomes larger. As mentioned before, we have taken $R_c = 10a$, which yields sufficient accuracy. We have taken n_{disks} in our simulations equal to 100 000, which is more than enough for the value $R_c = 10a$ that we have used. We note that n_{disks} should be taken to be much larger than n_{images} , because the potential of a disk-shaped charge distribution decays much slower with increasing distance than the potential of a point charge. The total contribution $e\Phi_{\text{disks},\mathbf{i}}$ is obtained by

$$e\Phi_{\text{disks},\mathbf{i}} = \sum_{j_x} e f_{\text{disk},i_x,j_x}. \quad (10)$$

Of particular interest is the spatial structure of the current density in the device. To investigate this structure we define at each site \mathbf{i} a local current $J_{\mathbf{i}}$ in the direction of the collecting electrode:

$$J_{\mathbf{i}} = e \frac{(f_{\mathbf{i}} - b_{\mathbf{i}})}{t_{\text{sim}}}, \quad (11)$$

with $f_{\mathbf{i}}$ ($b_{\mathbf{i}}$) the total number of forward (backward) hops from site \mathbf{i} in the direction of the collecting (injecting) electrode and t_{sim} the total simulation time. We note that we only allow hops over a maximum distance of $\sqrt{3}a$ (see Sec. III). Therefore, the forward (backward) hops are over a maximum distance of a in (against) the x direction. The total current density J_{i_x} in layer i_x is then given by

$$J_{i_x} = \sum_{i_y=1}^{m_y} \sum_{i_z=1}^{m_z} \frac{J_{\mathbf{i}}}{a^2 m_y m_z}, \quad (12)$$

where the summation is over all sites in the layer i_x parallel to the electrodes within the device. In a stationary situation, the current density J_{i_x} should be the same in each layer i_x .

Our simulations proceed as follows. We start with an empty device and apply the voltage V . We arbitrarily assume that the hopping carriers are positively charged. Hops of carriers are chosen with weights determined by the hopping rates given

by Eq.(1). For every hop, a hopping time is chosen from an exponential distribution with an inverse decay time equal to the sum of all possible hopping rates. After every hop the short-range Coulombic energy contribution $e\Phi_{\text{sr},\mathbf{i}}$ is updated for every site in the device to which another hop can occur. For practical reasons, the layer-averaged contributions $e\Phi_{\text{layer},\mathbf{i}}$ and $e\Phi_{\text{disks},\mathbf{i}}$ are only updated after every 100 hops. After a sufficiently long simulation time a stationary situation is obtained, as judged by monitoring the spread and the time dependence of the current densities J_{i_x} in the different layers i_x . After that the data gathering starts. The simulation ends when a sufficiently accurate current density J_{i_x} is obtained for every layer i_x . The final result for the current density is obtained after averaging over a number (typically 10 or 20) of disorder configurations. The relative accuracy of the resulting averaged current densities J is $\sim 10\%$.

B. One-dimensional continuum drift-diffusion model

We will compare the $J(V)$ curves obtained from the MC simulations described in the previous section to the $J(V)$ curves obtained from a 1D continuum drift-diffusion model. In this model the current density is given by the drift-diffusion equation

$$J = n(x)e\mu(x)F(x) - eD(x)\frac{dn(x)}{dx}, \quad (13)$$

with $n(x)$, $F(x)$, $\mu(x)$, and $D(x)$ the local charge-carrier density, the local electric field, the local mobility, and the local diffusion coefficient, respectively. $n(x)$ and $F(x)$ are related to each other via the Poisson equation, $dF/dx = (e/\epsilon_0\epsilon_r)n(x)$. The density, field, and temperature dependence of the local mobility $\mu(x) = \mu(n(x), F(x), T)$ is given by the EGDM or ECDM parametrization^{8,10} in the case of uncorrelated or correlated disorder, respectively. The local diffusion coefficient is obtained from the local mobility by using the generalized Einstein equation.³⁰

To solve the 1D drift-diffusion equation, the carrier densities at the electrode planes, n_c , are assumed to be constant

and given by the condition of thermal equilibrium between the electrode and the organic layer:

$$n_c = \int_{-\infty}^{\infty} \frac{g(E)}{1 + \exp\left[\frac{E+\Delta}{k_B T}\right]} dE. \quad (14)$$

The fact that disorder enhances injection by providing “hot spots” for injection at energetically low-lying sites is taken into account in an average way by the integral over the DOS in this equation. When the local field F_c at the electrode plane, as calculated by the external field V/L and by the Poisson equation, is negative, the local drift contribution of the current is directed toward the electrode. In this case we do not correct for the image potential. However, when the local field at the electrode plane is positive, the local drift contribution of the current is directed away from the injecting electrode. In this case we assume a thermal equilibrium between the electrode and the maximum of the total potential formed by the external potential V/L , the potential as calculated by the Poisson equation, and the image potential. As in Ref. 15 we make use of an image-charge-corrected barrier height, Δ' , in Eq. (14), as first suggested by Emtage and O'Dwyer,²⁰

$$\Delta' = \Delta - e \sqrt{\frac{e F_c}{4\pi\epsilon_0\epsilon_r}}, \quad (15)$$

where F_c and Δ' are determined self-consistently by using an iterative procedure. We note that because the electric field at the exit electrode is always directed toward this electrode, there is no correction for image-charge effects at this electrode.

The above approach of taking into account the effect of image charges suffers from a similar double-counting problem as the master-equation approach. For the case of Boltzmann statistics and the absence of disorder, the problem of taking into account the effect of image charges in a consistent way was recently discussed in detail by Genenko *et al.*²⁵ These authors delineate the regions of validity of what they call the “mean-field” (MF) and “single-particle” (SP) approach for varying injection barrier and local field at the electrodes. In the MF approach the effects of image charges are accounted for solely by the boundary conditions for the electrostatic potential at the electrodes, while in the SP approach only the explicit image potential of a single charge close to the electrodes is taken into account. The “modified mean-field” (MMF) approach proposed by these authors corresponds to Eq. (15), where the second term in this equation is multiplied by a prefactor that accommodates a smooth switch-on of the image-charge potential when passing the region of validity of the MF approach to the region of validity of the SP approach. The authors argue that the MMF approach more accurately treats injection for intermediate-sized injection barriers.

III. RESULTS FOR CURRENT-VOLTAGE CHARACTERISTICS

In Fig. 1 we display the room-temperature current density J in symmetric single-carrier devices with uncorrelated Gaussian disorder as a function of the applied voltage V , for different values of the injection barrier $\Delta = \Delta_1 = \Delta_2$. The open symbols indicate the results of MC simulations for the case

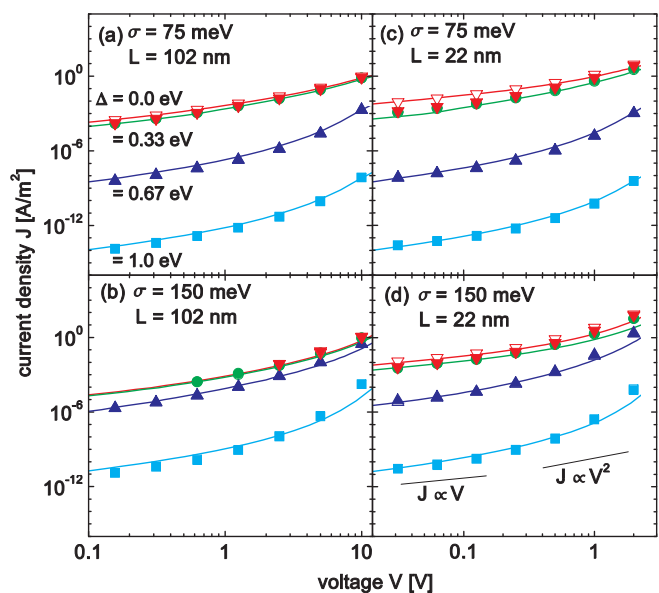


FIG. 1. (Color online) Dependence of the current density (J) on the driving voltage (V) for devices with an uncorrelated Gaussian DOS. The devices have thicknesses of $L = 102$ nm and $L = 22$ nm and disorder strengths of $\sigma = 75$ meV and $\sigma = 150$ meV, as indicated in (a)–(d). The results are for room temperature and a lattice constant $a = 1.6$ nm. The values used for the attempt-to-jump frequency, ν_0 in Eq.(1), are 3.5×10^{13} s $^{-1}$ for devices with $\sigma = 75$ meV and 1.4×10^{16} s $^{-1}$ for devices with $\sigma = 150$ meV. These values correspond to a mobility prefactor μ_0 (as defined in Ref. 8) equal to 4.8×10^{-14} m 2 /(V s) and 1.1×10^{-16} m 2 /(V s), respectively. Closed symbols: Results obtained from MCo simulations including short-range Coulomb interactions, for different injection barriers Δ : 0 eV (downward pointing triangles), 0.33 eV (circles), 0.67 eV (upward pointing triangles), and 1 eV (squares). In (b) no reliable results could be obtained for $\Delta = 0$ and 0.33 eV for the lower voltages. Open symbols: Results obtained from MC simulations without short-range Coulomb interactions. Solid lines: Results obtained from the 1D continuum drift-diffusion model as explained in the main text. A linear Ohmic dependence $J \propto V$ expected at low voltage is indicated, as well as a quadratic dependence $J \propto V^2$ expected for a space-charge-limited current with a constant mobility.

that short-range Coulomb interactions are neglected, which corresponds to setting the cutoff radius R_c of the sphere within which Coulomb interactions are taken into account explicitly equal to zero. The closed symbols correspond to the results of MC simulations for which the short-range contributions of the Coulomb interactions are taken into account ($R_c = 10a$, see Sec. II A). Results are given for four different values of the injection barrier, $\Delta = 0, 0.33, 0.67$, and 1 eV. The lattice constant is taken to be equal to $a = 1.6$ nm, a value found in Ref. 8 from modeling the transport in a hole-only device based on the PPV derivative OC $_1$ C $_{10}$ -PPV (poly[2-methoxy-5-(3',7'-dimethyloctyloxy)-*p*-phenylene vinylene]). We choose $\alpha = 10/a$ in Eq.(1) and allow for hops over a maximum distance of $\sqrt{3}a$, as in our calculations with the master-equation approach.¹⁵ The four plots in Fig. 1 show results for two different values of the disorder strength, $\sigma = 3k_B T$ [Figs. 1(a) and 1(c)] and $6k_B T$ [Figs. 1(b) and 1(d)], which correspond to room temperature to $\sigma = 75$ and 150 meV,

respectively. Two device thicknesses are taken, $L = 22.4$ nm [13 layers, Figs. 1(c) and 1(d)] and 102.4 nm [63 layers, Figs. 1(a) and 1(b)], which are denoted by “22 nm” (“thin”) and “102 nm” (“thick”), respectively. The lateral grid size is 50×50 sites, which is sufficiently large. The relative dielectric constant ϵ_r is taken to be equal to 3, as in Ref. 8. The attempt-to-jump frequency, ν_0 , is chosen in such a way that the current density as obtained from the simulations is equal to 1 A/m^2 for the thick device at $V = 10 \text{ V}$, for the case where $R_c = 0$. The value of ν_0 is then equal to 3.5×10^{13} and $1.4 \times 10^{16} \text{ s}^{-1}$ in the case of a device with a disorder strength $\sigma = 3k_B T$ and $6k_B T$, respectively. We were not able to obtain sufficiently accurate results for the 102-nm device in the case of a disorder strength $\sigma = 6k_B T$ for the lowest injection barriers and voltages [Fig. 1(b)].

We find that the results obtained without taking into account short-range Coulomb interactions are virtually indistinguishable from the results obtained by the master-equation calculations of exactly the same devices in Ref. 15. Because the master equation is an equation for the time-averaged occupational probabilities of the sites, it is not possible to include Coulomb interactions explicitly in these calculations. Another aspect of the master-equation calculations is that correlations between occupational probabilities of sites are not accounted for, whereas such correlations are taken into account in the MC simulations (even if short-range Coulomb interactions are not accounted for). By taking into account correlations between the occupational probabilities of pairs of neighboring sites, it was shown that the effect of such correlations on the current is very small.³¹ This is in agreement with the observed indistinguishability between the master-equation results and the MC results without short-range Coulomb interactions. We do not plot the results of the master-equation calculations in Fig. 1, because these essentially coincide with the open symbols shown in Fig. 1.

The drawn lines in Fig. 1 correspond to results obtained from the 1D drift-diffusion model described in Sec. II B. These results follow the MC results without short-range Coulomb interactions quite accurately, except for the thin device ($L = 22$ nm) with strong disorder ($\sigma = 6k_B T$) at voltages higher than 1 V [Fig. 1(d)]. These observations are equivalent to those made in Ref. 15.

For the lower injection barriers ($\Delta = 0$ and 0.33 eV) the devices are in the space-charge-limited current (SCLC) regime and the current density almost does not depend on the size of the injection barrier. In devices with weak disorder ($\sigma = 3k_B T$) the current density is dependent on the injection barrier for the higher injection barriers ($\Delta = 0.67$ and 1.0 eV). In this case the devices are in the injection-limited current (ILC) regime. For devices with strong disorder ($\sigma = 6k_B T$), the current density is still dominated by space-charge effects at an injection barrier of $\Delta = 0.67$ eV, because the higher disorder leads to a higher carrier density close to the electrodes as compared to the devices with $\sigma = 3k_B T$, owing to the larger filling of the states in the tail of the Gaussian DOS. For high injection barriers the current density in the 22- and 102-nm devices is almost the same for equal injection barriers if the voltage is scaled with the device thickness.

The most important observation to be made, however, is that for devices without injection barrier ($\Delta = 0$ eV),

the current density resulting from the MC simulations with short-range Coulomb interactions is considerably lower than the current density resulting from the simulations without these interactions (and also considerably lower than the 1D drift-diffusion results). For the thin device ($L = 22$ nm) with weak disorder ($\sigma = 3k_B T$) the current density with short-range interactions is at $V = 2 \text{ V}$, $\sim 25\%$ lower than without short-range interactions [Fig. 1(c)]. This difference increases for lower voltages to a factor of ~ 6 . The difference is less for devices with a higher disorder strength [a factor of ~ 3 for the thin device with $\sigma = 6k_B T$ at low voltages; see Fig. 1(d)] and a larger thickness [a factor of ~ 2 for the thick device with $\sigma = 3k_B T$ at low voltages; see Fig. 1(a)]. When short-range Coulomb interactions are taken into account, the current density in devices with no injection barrier is almost the same as the current density in a device with an injection barrier $\Delta = 0.33$ eV. Hence, the effect of taking into account short-range Coulomb interactions is similar to the effect of an increase of the injection barrier. By analyzing the dependence of the current density on the injection barrier, we found that at approximately $\Delta = 0.3$ eV the difference between the MC results with and without short-range Coulomb interactions disappears. This means that for injection barriers higher than ~ 0.3 eV the density of carriers in the device becomes so low that short-range Coulomb interactions have no influence anymore.

The saturation of the current with decreasing injection barrier at an injection barrier of ~ 0.3 eV is reminiscent of the pinning of the injection barrier by the transfer of charge from the electrode to the first organic layer under the influence of the image potential, leading to the formation of a dipole layer, as described by Tutiš *et al.*³² In this way these authors try to explain the experimentally observed pinning of the injection barrier for devices of tris(8-hydroxyquinolinato) aluminum (Alq_3) at ~ 0.6 eV with low work-function metals.³³ However, the distance between the electrode and the first organic layer assumed by Tutiš *et al.* is 0.3 nm and hence it is much smaller than the value of 1.6 nm assumed by us, so that this mechanism of pinning of the injection barrier would occur at much lower injection barriers in our case. We explicitly checked that the difference in charge transfer to the first organic layer for the situation with and without Coulomb interactions is not enough to yield an injection barrier difference of 0.3 eV, so that another mechanism should be responsible for the difference in the current between the situation with and without short-range Coulomb interactions. We will try to identify this mechanism in what follows.

In Fig. 2 we display similar results as in Fig. 1, but now for the case of dipole-correlated disorder. Correspondingly, the 1D drift-diffusion calculations were performed with the ECDM mobility function.¹⁰ The attempt-to-jump frequency is chosen in a similar way as in Fig. 1, leading to $\nu_0 = 9.5 \times 10^{12}$ and $4.8 \times 10^{13} \text{ s}^{-1}$ in the case of disorder strengths $\sigma = 3k_B T$ and $6k_B T$, respectively. For the 102-nm device in the case of a disorder strength $\sigma = 6k_B T$ and injection barrier $\Delta = 0$, we could not obtain an accurate result at the lowest voltage [Fig. 2(b)].

The agreement between the MC results without short-range Coulomb interactions and the 1D drift-diffusion results is somewhat worse than in the case of uncorrelated disorder,

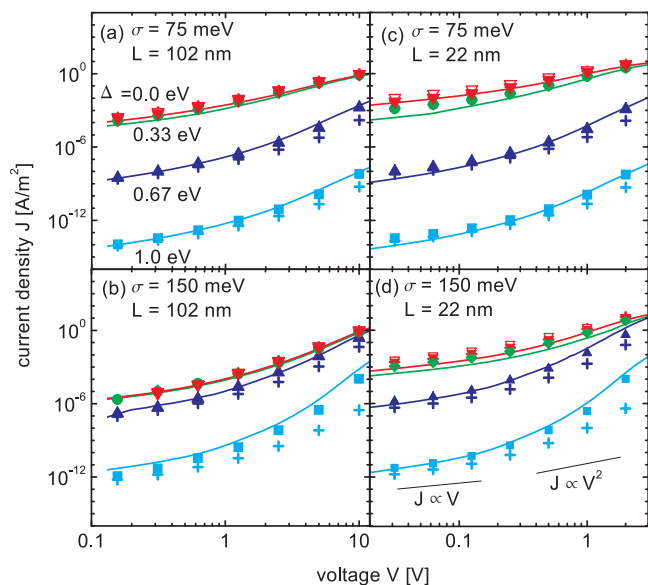


FIG. 2. (Color online) The same as in Fig. 1, but for correlated disorder. The values used for the attempt-to-jump frequency, ν_0 in Eq.(1), are $9.5 \times 10^{12} \text{ s}^{-1}$ for devices with $\sigma = 75 \text{ meV}$ and $4.8 \times 10^{13} \text{ s}^{-1}$ for devices with $\sigma = 150 \text{ meV}$. These values correspond to a mobility prefactor μ_0 (as defined in Ref. 10) equal to $2.4 \times 10^{-14} \text{ m}^2/(\text{V s})$ and $2.4 \times 10^{-17} \text{ m}^2/(\text{V s})$, respectively. In (b) no reliable results could be obtained for $\Delta = 0$ at the lowest voltage. The + symbols indicate the results for the case where image dipoles in the electrodes are taken into account.

especially for thin devices, high disorder strengths, low applied voltages, and low injection barriers. For low injection barriers ($\Delta = 0$ and 0.33 eV) the current is again space-charge limited. For both disorder strengths $\sigma = 3k_B T$ and $6k_B T$ and at high injection barriers $\Delta = 0.67$ and 1.0 eV the devices are injection limited.

We have also plotted in Fig. 2 the results for the case that the correlated disorder is obtained by taking into account image dipoles in the electrodes (+ symbols). The effect of these image dipoles is to reduce the disorder close to the electrodes.³⁴ This leads to a reduced current, because the effect of enhanced injection into energetically low-lying states in the organic material³⁵ is less. This reduction only occurs for high injection barriers. As the results of the MC simulations with and without short-range Coulomb interactions are coinciding for high injection barriers, we only show the former results. For an injection barrier $\Delta = 1.0 \text{ eV}$, a voltage $V = 2 \text{ V}$, and device thickness $L = 22 \text{ nm}$, the current is decreased by a factor of ~ 10 and 300 in the case of disorder strengths $\sigma = 75$ and 150 meV , respectively. In the case of $L = 102 \text{ nm}$ the current is decreased by a factor of ~ 10 and 400 , respectively. For low injection barriers the reduction of the current by image dipoles is insignificant because the current is then limited by space charge and not by injection. In the remainder of the paper we will not take into account the effects of image dipoles when discussing results for correlated disorder.

The difference between the results of the MC simulations with short-range Coulomb interactions and those without short-range Coulomb interactions are now smaller than for the case of uncorrelated disorder. The current density in the

thin device with weak disorder [Fig. 2(c)] with short-range Coulomb interactions is at $V = 2 \text{ V}$, only $\sim 10\%$ lower than without short-range Coulomb interactions. This difference increases for lower voltages to a factor of ~ 2 . The difference is almost negligible in the thick device [Figs. 2(a) and 2(b)] and at high disorder strength [Fig. 2(d)]. We note that the difference between the current-voltage characteristics with and without short-range Coulomb interactions occurs at very small injection barriers, as shown in Fig. 1 for the case $\Delta = 0$. The effect occurs thus in the MF regime (within the terminology used by Genenko *et al.*²⁵), within which the electric field is directed toward the electrode. The MMF approach of Genenko *et al.*, which applies to intermediate energy barriers resulting in a positive field, is then inapplicable. At the nonzero injection barriers that we studied, the double-counting error made in the master-equation approach and in the 1D drift-diffusion modeling apparently does not lead to any significant error.

An important conclusion is that the current with short-range Coulomb interactions included is in our simulations always *smaller* than without short-range Coulomb interactions. This conclusion appears to be at odds with the conclusion of Zhou *et al.*,²² that Coulomb interactions decrease the mobility at low disorder strength but increase the mobility at high disorder strength. However, this conclusion was drawn from results obtained at a rather large electric field of $F = 4kT/ea$, a field strength that is only reached at the highest voltages in Figs. 1 and 2. The reduction of the current found by us is compatible with the theoretical prediction of a Coulomb gap opening up around the Fermi energy in the DOS of a system of interacting localized charges,^{36,37} which leads to a reduction of the carrier mobility at low electric field.

IV. EFFECTS OF SHORT-RANGE COULOMB INTERACTIONS ON THE THREE-DIMENSIONAL CURRENT DISTRIBUTIONS

In this section we show the 3D current distributions in the devices with and without taking into account short-range Coulomb interactions. From the structure of these distributions we will try to rationalize the trends in the effects of short-range interactions on the total current observed in the previous section. Figure 3 shows the time-averaged 3D current distributions, calculated with Eq. (11), at room temperature of a thin device of $L = 22 \text{ nm}$ for uncorrelated disorder with a disorder strength of $\sigma = 3k_B T$ [Figs. 3(a) and 3(b)] and $\sigma = 6k_B T$ [Figs. 3(c)–3(f)] at an applied voltage of $V = 0.5 \text{ V}$. Figures 3(a)–3(d) show the results without an injection barrier, while Figs. 3(e) and 3(f) show the results for $\sigma = 6k_B T$ with an injection barrier of $\Delta = 1 \text{ eV}$. In Figs. 3(a), 3(c), and 3(e) short-range Coulomb interactions have not been taken into account, while these have been taken into account in Figs. 3(b), 3(d), and 3(f). Apart from a factor of 2 difference in the energies between $\sigma = 3k_B T$ and $\sigma = 6k_B T$, exactly the same disorder configuration of the random energies of the organic sites has been taken in Figs. 3(a)–3(f). Figure 4 shows the same results for correlated disorder (without taking into account the effects of image dipoles).

As already noted in Ref. 15 the energetic disorder leads to a strong filamentary structure of the current distribution,

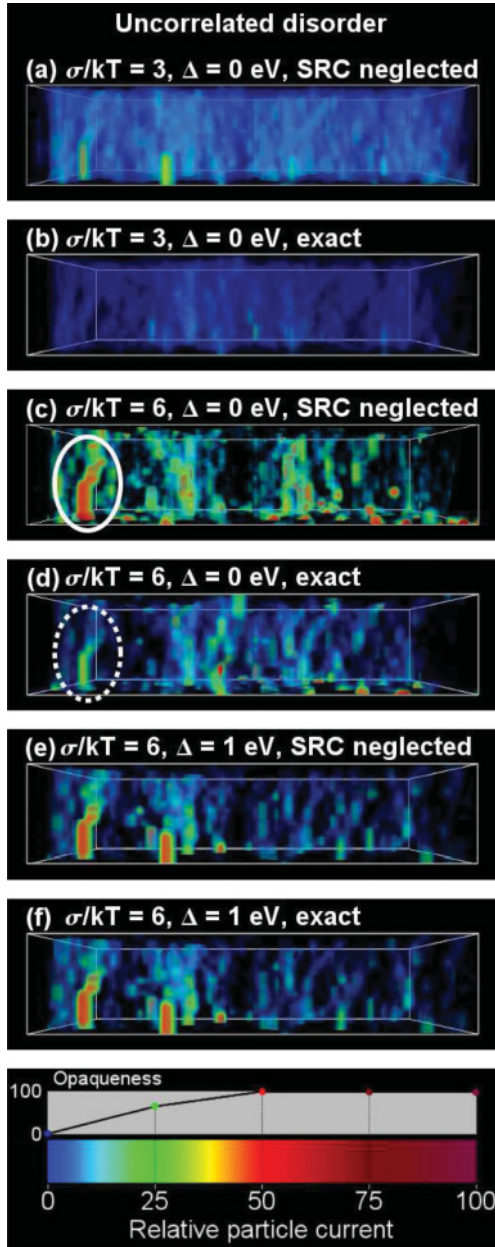


FIG. 3. (Color online) 3D representation of the relative local current density in the direction of the applied field, given by $J_{rel,i} = J_i/J_{av}$, with J_i the absolute local current density given by Eq. (11). The displayed results are for devices with uncorrelated disorder, device thickness $L = 22$ nm, driving voltage $V = 0.5$ V, room temperature, and lattice constant $a = 1.6$ nm. In all representations (a)–(f) the device is viewed from the side with the injecting electrode at the bottom. The energetic disorder configurations of the organic sites are all the same, apart from a factor of 2 difference in energies between $\sigma = 75$ and 150 meV. In (a), (c), and (e) short-range Coulomb (SRC) interactions have not been included, while these have been included in (b), (d), and (f). The local current density is coded with a color and transparency, with the coding scheme indicated at the bottom. The normalization J_{av} is in each case the average local current density in the device if short-range Coulomb interactions are included. The lateral grid size used is 50×50 sites. The boundaries of the device are depicted by a white bounding box. The circles with full and dotted lines indicate regions where the blocking effect by short-range Coulomb interactions occurs.

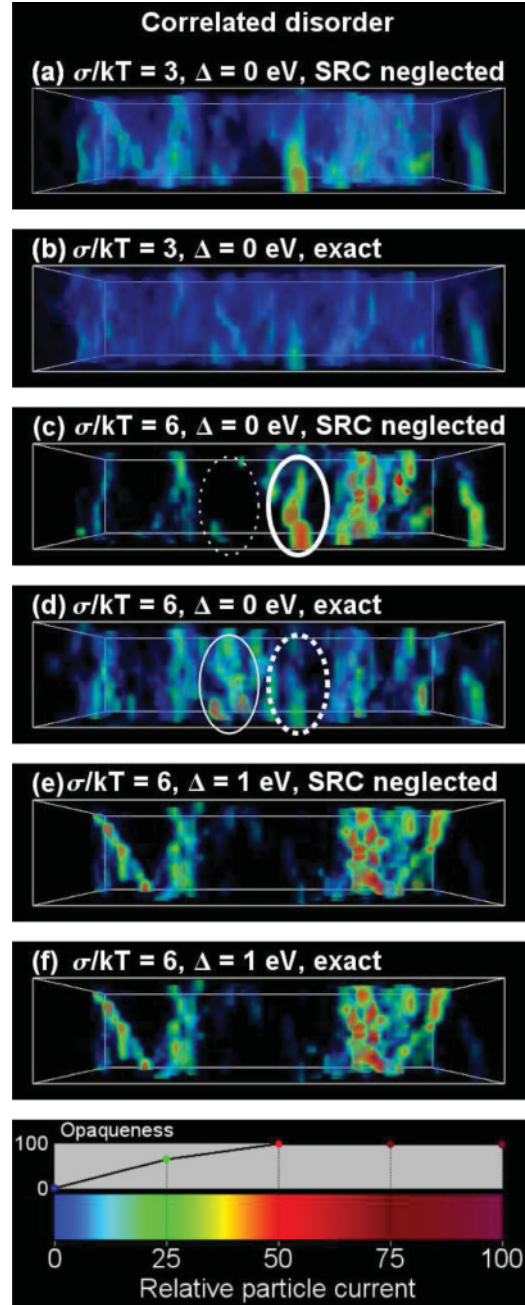


FIG. 4. (Color online) The same as in Fig. 3, but for correlated disorder. The circles with thick full and dotted lines indicate regions where the blocking effect by short-range Coulomb interactions occurs, whereas the circles with thin full and dotted lines indicate regions where the declotting effect by short-range Coulomb interactions occurs.

because of the percolative character of the charge transport. In the case of vanishing injection barrier $\Delta = 0$ there is a significant effect of short-range Coulomb interactions on the current distributions [compare Figs. 3(a) and 3(b), Figs. 3(c) and 3(d), Figs. 4(a) and 4(b), and Figs. 4(c) and 4(d)]. In the case of uncorrelated disorder the inclusion of short-range Coulomb interactions almost always leads to a local decrease of the current density. The reason for this is that the short-range Coulomb interactions prevent carriers from always following

the most favorable percolating path from one electrode to the other, because a trapped carrier close to a percolating path may temporarily block that path by repelling other carriers. The circles in Figs. 3(c) and 3(d) indicate regions where this effect occurs. This leads to the reduction of the current as described in the previous section. We remark that with growing disorder the strength of the Coulomb interactions ($e\Phi_{\text{interact},i}$) to the on-site energy of a charge as compared to the random contribution ($E_{\text{rand},i}$) becomes less important. Conversely, this means that, although the filamentary structure for $\sigma = 3k_B T$ is less pronounced than for $\sigma = 6k_B T$, the relative effect of short-range Coulomb interactions as compared to the energetic disorder is larger. This explains the relatively stronger reduction of the current by short-range Coulomb interactions for weaker disorder found in the previous section.

On the other hand, in the case of an injection barrier of $\Delta = 1.0$ eV, there is no observable effect of short-range Coulomb interactions on the current distributions [compare Figs. 3(e) and 3(f) and Figs. 4(e) and 4(f)], in line with the absence of an effect on the current-voltage characteristics in Figs. 1 and 2. The absence of an effect of short-range Coulomb interactions on the current distribution for this relatively high injection barrier is related to the very low carrier density in the device. We note that for an applied voltage of 2 V we could for $\sigma = 6k_B T$ very accurately reproduce the current distribution obtained with the master-equation approach shown in Fig. 3(c) in Ref. 15 for the case of uncorrelated disorder, using the same disorder configuration as in that work. This is in line with the observation made in the previous section that the current-voltage characteristics obtained from the MC simulations without short-range Coulomb interactions are indistinguishable from those obtained from the master-equation calculations in Ref. 15. Although we do not show the current distributions for the case of $\sigma = 3k_B T$ and an injection barrier of $\Delta = 1.0$ eV, these conclusions also hold for that case.

For the case of correlated disorder we observe that the filamentary structure of the current is different than for uncorrelated disorder. The current filaments are now typically broader than for uncorrelated disorder [this is in particular clearly visible in the right-hand parts of Figs. 4(d)–4(f)]. The reason is that, owing to the spatial energetic correlation, the percolating paths acquire a width that is broader than the single lattice spacing that is typical for the case of uncorrelated disorder. We now observe two opposing effects on the current distribution. In some regions, the inclusion of short-range Coulomb interactions leads to a decrease of the local current, as in the case of uncorrelated disorder. The circles with thick lines in Figs. 4(c) and 4(d) indicate regions where this effect occurs. However, in other regions, including short-range Coulomb interactions, this leads to an *increase* of the current, owing to a “declotting effect” that will be explained below. The circles with thin lines in Figs. 4(c) and 4(d) indicate regions where this opposing effect occurs. The partial cancellation of these two opposing effects explains the observation in the previous section that the effect of short-range Coulomb interactions on the total current is, in the case of correlated disorder, smaller than in the case of uncorrelated disorder.

In order to further investigate the effects of short-range Coulomb interactions we plot in Fig. 5 the in-plane radial

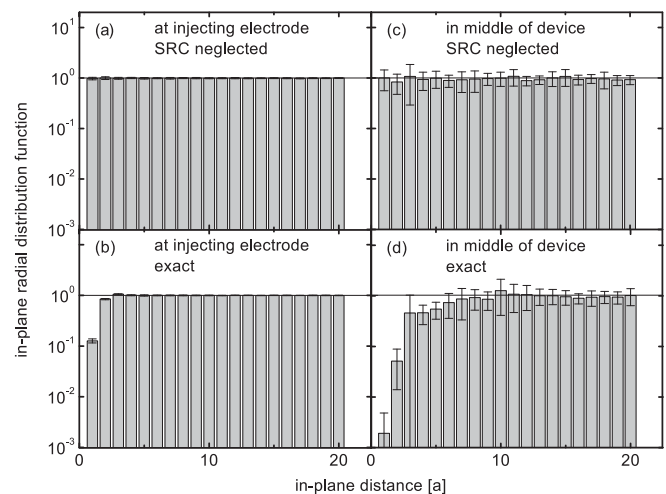


FIG. 5. In-plane radial distribution functions for a device thickness $L = 22$ nm, driving voltage $V = 0.5$ V, room temperature, injection barrier $\Delta = 0$, lattice constant $a = 1.6$ nm, $\sigma = 75$ meV, and uncorrelated disorder. (a) and (c) Without short-range Coulomb interactions. (b) and (d) With short-range Coulomb interaction. (a) and (b) In the first organic layer at the injecting electrode. (c) and (d) In the middle of the device. The layer charge densities in the different graphs are (a) 0.093, (b) 0.051, (c) 0.000 57, and (d) 0.0011 carriers per site. Results are shown for averages over 10–30 disorder configurations. The error bars are indicated.

distribution functions for the case of uncorrelated disorder, excluding [Figs. 5(a) and 5(c)] and including [Figs. 5(b) and 5(d)] short-range Coulomb interactions, in the first organic layer at the injection electrode [Figs. 5(a) and 5(b)] and in the middle layer of the device [Figs. 5(c) and 5(d)]. These distribution functions are a measure for the probability to find pairs of carriers at a certain distance from each other in a layer (a value of 1 means that no correlation exists). The plots have been made for the case where the effect of short-range Coulomb interactions is most pronounced: $\Delta = 0$, $\sigma = 75$ meV, and $L = 22$ nm. We clearly see that the effect of taking into account short-range Coulomb interactions is to reduce the probability to find two charges close to each other. In the first organic layer, the radial distribution function with short-range Coulomb interactions taken into account reaches unity at a distance of $\sim 4a$. With a density of 0.093 carriers per site in this layer the average distance between the carriers is $0.093^{-1/3}a \approx 2.2a$, meaning that the effects of short-range Coulomb interactions are very significant. In the middle layer, the distribution function reaches unity at a larger distance. The reason is that, with a much smaller density of 0.000 57 carriers per site in this layer, the screening effects are smaller. The average distance between carriers is $0.000 57^{-1/3}a \approx 12a$ in this layer. At this distance the distribution function has reached unity, so that the effects of short-range Coulomb interactions are smaller in this layer. We also investigated the distribution functions in the last organic layer at the collecting electrode and found that these are quite similar to those in the first organic layer.

The corresponding results for correlated disorder are shown in Fig. 6. We note that in this case the radial distribution functions strongly deviate from unity already without including

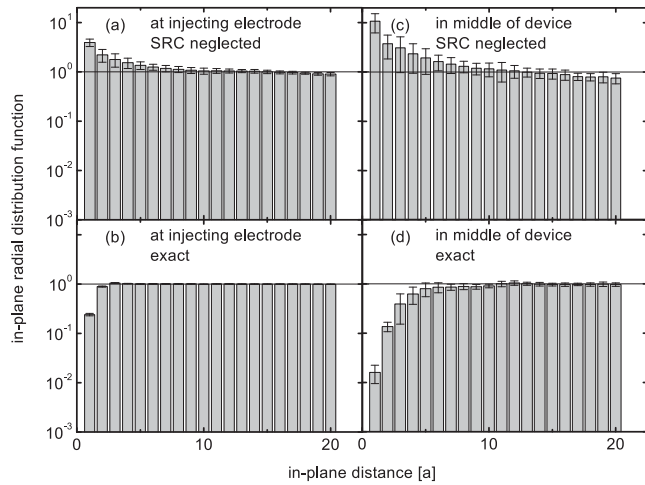


FIG. 6. The same as in Fig. 6, but for correlated disorder, with layer charge densities of (a) 0.078, (b) 0.049, (c) 0.0014, and (d) 0.0013 carriers per site.

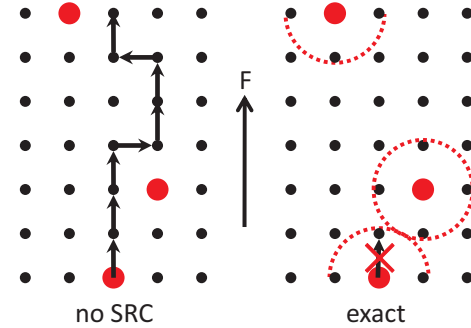
Coulomb interactions [see Figs. 6(a) and 6(c)]. The reason is that the spatial correlation in the site energies leads to an enhanced probability that two charges are found close together. The inclusion of short-range Coulomb interactions reverses this situation [see Figs. 6(b) and 6(d)]. In this case the distribution functions look qualitatively similar to those for uncorrelated disorder [Figs. 5(b) and 5(d)]. A quantitative difference is that for correlated disorder the distribution functions deviate less from unity than for uncorrelated disorder. This is caused by the opposing effects of the spatial correlation in the site energies and the short-range Coulomb interactions.

The above results for the radial distribution functions help us to understand the effects of short-range Coulomb interactions on the current distributions. These effects are indicated in a cartoonlike fashion in Fig. 7. We distinguish a “blocking effect” [Fig. 7(a)] and a “declotting effect” [Fig. 7(b)]. In the blocking effect, which was already discussed above, the short-range Coulomb interactions of carriers that are deeply trapped in the DOS block certain pathways for the mobile carriers. In the case of correlated disorder, however, an opposing effect also occurs. In the absence of short-range Coulomb interactions, “clots” of carriers in energetically low-lying sites occur. These clots lead to a radial distribution function that is larger than unity at short distances [see Figs. 6(a) and 6(c)]. Within the clots, the motion of carriers is blocked because of the fact that only one carrier can occupy a site. The short-range Coulomb interactions cause a declotting by repulsion of carriers, leading to a radial distribution function that is smaller than unity at short distances [see Figs. 6(b) and 6(d)]. Because of this declotting, carriers are more free to move. Blocking and declotting effects may dominate in different regions, which is observed in Figs. 4(a)–4(d), as already noted above.

V. SUMMARY AND CONCLUSIONS

By performing 3D MC simulations, we have studied single-carrier transport in devices consisting of an organic semicon-

(a) blocking by Coulomb interactions
uncorrelated or correlated disorder



(b) declotting by Coulomb interactions
correlated disorder

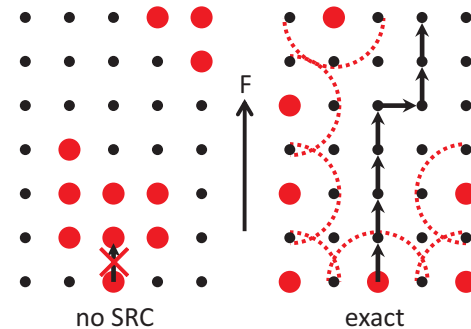


FIG. 7. (Color online) The two effects explaining the difference in the 3D current density distribution for the case where short-range Coulomb interactions are not included (no SRC) and the case where they are included (exact). The dotted circles indicate the Coulomb repulsion of the carriers. The electric field F is indicated. (a) In the blocking effect, carriers that are trapped in energetically low-lying sites block the motion of mobile carriers by short-range Coulomb interactions. (b) In the declotting effect, occurring in the case of correlated disorder, the short-range Coulomb interactions break up clots of carriers that exist when these interactions are not included. Carriers are then more free to move.

ductor sandwiched in between two metallic electrodes, for the cases of uncorrelated Gaussian energetic disorder in the organic semiconductor as well as correlated Gaussian energetic disorder caused by the electrostatic field of random dipoles. In particular, the effects of Coulomb interactions between the carriers were studied. Up to now, in device modeling studies, only the long-range effects of Coulomb interactions have been included through the space-charge potential. We studied the situations with and without inclusion of short-range Coulomb interactions. We also varied the injection barrier between the electrodes and the organic semiconductor. The effects of image charges in the electrodes were fully taken into account.

For the case of uncorrelated disorder we found that, with an injection barrier of ~ 0.3 eV or higher, for the devices we studied, it is not necessary to include the short-range Coulomb interactions, because of the low carrier density in the devices. Our results for the current-voltage characteristics are then in accurate agreement with previous calculations by us of the

same devices with a master-equation approach, in which the Coulomb interactions between the charges were taken into account in a layer-averaged way.¹⁵ This also means that the way we have taken into account image charges in Ref. 15, which suffers from a double-counting problem owing to the fact that image charges have also been taken into account in a layer-averaged way via the space charge, does not lead to significant errors for these injection barriers. Our results for the current are then also in good agreement with 1D drift-diffusion calculations with a mobility function based on the EGDM,⁸ in which the dependence of the mobility on temperature, electric field, and carrier density is taken into account.

If the injection barrier in the case of uncorrelated disorder is smaller than 0.3 eV, however, the inclusion of short-range Coulomb interactions leads to a significant reduction of the current. By analyzing the 3D current distribution, we attributed this to the fact that the short-range Coulomb interactions change the filamentary structure of this distribution, where favorable percolating pathways for the current are partially blocked. We investigated the blocking effect of short-range Coulomb interactions by analyzing the in-plane radial distribution functions with and without including short-range Coulomb effects. The reduction of the current is larger for smaller disorder strength owing to the relatively larger importance of Coulomb interactions in that case. The difference between current-voltage characteristics with and without taking into account short-range Coulomb interactions should not be attributed to the double-counting problem because the image-charge contribution to the potential then does not appear in the 1D drift-diffusion calculations.

For the case of correlated disorder we found similar results, with the important difference that the short-range Coulomb interactions lead to a smaller reduction of the current at a vanishing injection barrier than for uncorrelated disorder. We explain this by the occurrence of a declotting effect that can

locally lead to an increase of the current, opposing the blocking effect. For not too small injection barriers we found a fair agreement between our 3D MC results for the current and 1D drift-diffusion calculations with a mobility function based on the ECDM.¹⁰ For high injection barriers, the inclusion of image dipoles causes a decrease of the current, owing to a decrease of the disorder close to the electrodes, which leads to a reduced injection into energetically low-lying states.

The relevance of the present work for the modeling of OLEDs is that the conventional drift-diffusion modeling approach can be applied in the transport for not too small injection barriers, when the effects of short-range Coulomb interactions can be neglected. In the case of small injection barriers, the effects of short-range Coulomb interactions become important, as demonstrated in the present work, but there is presently no systematic and simple theory to include these effects. We note that we have recently shown that in order to properly describe electron-hole recombination in double-carrier devices, it is also necessary to take into account the effects of short-range interactions.³⁸ If these interactions are included in the mobilities in a double-carrier situation, an accurate description of the recombination rate is found when these mobilities are used in the conventional Langevin expression for this rate.³⁸ It would therefore be highly desirable to develop a systematic theory for including short-range Coulomb effects on charge-carrier mobilities in disordered organic semiconductors.

ACKNOWLEDGMENTS

This research was supported by NanoNed, a national nanotechnology program coordinated by the Dutch Ministry of Economic Affairs (J.J.M.v.d.H.), and by the European Community's Seventh Framework programme (Grant agreement 213708, AEVIOM, F.W.A.v.O, R.C., and P.A.B.).

*j.j.m.v.d.holst@tue.nl

¹L. Pautmeier, R. Richert, and H. Bässler, *Synth. Met.* **37**, 271 (1990).

²H. Bässler, *Phys. Status Solidi B* **175**, 15 (1993).

³Y. N. Gartstein and E. M. Conwell, *Chem. Phys. Lett.* **245**, 351 (1995).

⁴D. H. Dunlap, P. E. Parris, and V. M. Kenkre, *Phys. Rev. Lett.* **77**, 542 (1996).

⁵S. V. Novikov, D. H. Dunlap, V. M. Kenkre, P. E. Parris, and A. V. Vannikov, *Phys. Rev. Lett.* **81**, 4472 (1998).

⁶Z. G. Yu, D. L. Smith, A. Saxena, R. L. Martin, and A. R. Bishop, *Phys. Rev. Lett.* **84**, 721 (2000).

⁷Y. Roichman and N. Tessler, *Synth. Met.* **135**, 443 (2003).

⁸W. F. Pasveer, J. Cottaar, C. Tanase, R. Coehoorn, P. A. Bobbert, P. W. M. Blom, D. M. de Leeuw, and M. A. J. Michels, *Phys. Rev. Lett.* **94**, 206601 (2005).

⁹S. L. M. van Mensfoort, S. I. E. Vulto, R. A. J. Janssen, and R. Coehoorn, *Phys. Rev. B* **78**, 085208 (2008).

¹⁰M. Bouhassoune, S. L. M. van Mensfoort, P. A. Bobbert, and R. Coehoorn, *Org. Electron.* **10**, 437 (2009).

¹¹R. J. de Vries, S. L. M. van Mensfoort, V. Shabro, S. I. E. Vulto, R. A. J. Janssen, and R. Coehoorn, *Appl. Phys. Lett.* **94**, 163307 (2009).

¹²S. L. M. van Mensfoort, V. Shabro, R. J. de Vries, R. A. J. Janssen, and R. Coehoorn, *J. Appl. Phys.* **107**, 113710 (2010).

¹³S. L. M. van Mensfoort, R. J. de Vries, V. Shabro, H. P. Loebel, R. A. J. Janssen, and R. Coehoorn, *Org. Electron.* **11**, 1408 (2010).

¹⁴S. L. M. van Mensfoort and R. Coehoorn, *Phys. Rev. B* **78**, 085207 (2008).

¹⁵J. J. M. van der Holst, M. A. Uijtewaald, B. Ramachandran, R. Coehoorn, P. A. Bobbert, G. A. de Wijs, and R. A. de Groot, *Phys. Rev. B* **79**, 085203 (2009).

¹⁶Z. G. Yu, D. L. Smith, A. Saxena, R. L. Martin, and A. R. Bishop, *Phys. Rev. B* **63**, 085202 (2001).

¹⁷E. Tutiš, I. Batistić, and D. Berner, *Phys. Rev. B* **70**, 161202(R) (2004).

¹⁸K. D. Meisel, W. F. Pasveer, J. Cottaar, C. Tanase, R. Coehoorn, P. A. Bobbert, P. W. M. Blom, D. M. de Leeuw, and M. A. J. Michels, *Phys. Status Solidi C* **3**, 267 (2006).

- ¹⁹J. J. Kwiatkowski, J. Nelson, H. Li, J. L. Bredas, W. Wenzel, and C. Lennartz, *Phys. Chem. Chem. Phys.* **10**, 1852 (2008).
- ²⁰P. R. Emtage and J. J. O'Dwyer, *Phys. Rev. Lett.* **16**, 356 (1966).
- ²¹A. L. Burin and M. A. Ratner, *J. Chem. Phys.* **113**, 3941 (2000).
- ²²J. Zhou, Y. C. Zhou, J. M. Zhao, C. Q. Wu, X. M. Ding, and X. Y. Hou, *Phys. Rev. B* **75**, 153201 (2007).
- ²³H. Houili, E. Tutiš, I. Batistić, and L. Zuppiroli, *J. Appl. Phys.* **100**, 033702 (2006).
- ²⁴J. Nelson, *Phys. Rev. B* **67**, 155209 (2003).
- ²⁵Y. A. Genenko, S. V. Yampolskii, C. Melzer, K. Stegmaier, and H. von Seggern, *Phys. Rev. B* **81**, 125310 (2010).
- ²⁶A. Miller and E. Abrahams, *Phys. Rev.* **120**, 745 (1960).
- ²⁷S. V. Novikov and A. V. Vannikov, *Sov. Phys. JETP* **79**, 482 (1994).
- ²⁸R. H. Young, *Philos. Mag. B* **72**, 435 (1995).
- ²⁹S. V. Novikov and A. V. Vannikov, *J. Phys. Chem.* **99**, 14573 (1995).
- ³⁰Y. Roichman and N. Tessler, *Appl. Phys. Lett.* **80**, 1948 (2002).
- ³¹J. Cottaar and P. A. Bobbert, *Phys. Rev. B* **74**, 115204 (2006).
- ³²E. Tutiš, M. N. Bussac, and L. Zuppiroli, *Appl. Phys. Lett.* **75**, 3880 (1999).
- ³³I. H. Campbell and D. L. Smith, *Appl. Phys. Lett.* **74**, 561 (1999).
- ³⁴S. V. Novikov, *Phys. Status Solidi C* **5**, 750 (2008).
- ³⁵V. I. Arkhipov, E. V. Emelianova, Y. H. Tak, and H. Bässler, *J. Appl. Phys.* **84**, 848 (1998).
- ³⁶M. Pollak, *Discuss. Faraday Soc.* **50**, 13 (1970).
- ³⁷A. L. Efros and B. I. Shklovskii, *J. Phys. C* **9**, 2021 (1976).
- ³⁸J. J. M. van der Holst, F. W. A. van Oost, R. Coehoorn, and P. A. Bobbert, *Phys. Rev. B* **80**, 235202 (2009).